

U₂Ni₂Sn and the origin of magnetic anisotropy in uranium compounds

S. Mašková,¹ A. V. Andreev,² Y. Skourski,³ S. Yasin,^{3,4} D. I. Gorbunov,³ S. Zherlitsyn,³ H. Nakotte,⁵ K. Kothapalli,^{5,6} F. Nasreen,⁷ C. Cupp,⁶ H. B. Cao,⁸ A. Kolomiets,^{1,9} and L. Havela¹

¹*Department of Condensed Matter Physics, Charles University, 12116 Prague, Czech Republic*

²*Institute of Physics, Academy of Sciences, 18221 Prague, Czech Republic*

³*Hochfeld-Magnetlabor Dresden (HLD-EMFL), Helmholtz-Zentrum Dresden-Rossendorf, 01328 Dresden, Germany*

⁴*College of Engineering and Technology, American University of the Middle East, Kuwait*

⁵*Department of Physics, New Mexico State University, Las Cruces, New Mexico 88003-8001, USA*

⁶*College of Arts and Sciences, King University, Bristol, Tennessee 37620, USA*

⁷*High Pressure Science and Engineering Center (HiPSEC) and Department of Physics and Astronomy, University of Nevada, Las Vegas, Nevada 89154, USA*

⁸*Neutron Scattering Division, Oak Ridge National Laboratory, Oak Ridge, Tennessee 37831, USA*

⁹*Department of Physics, Lviv Polytechnic National University, 79013 Lviv, Ukraine*

U₂Ni₂Sn is a member of a large family of intermetallic compounds with the tetragonal Mo₂FeB₂ crystal structure. It orders antiferromagnetically at 25 K with propagation vector $q = (0, 0, \frac{1}{2})$. Magnetization, magnetoacoustic, and neutron-diffraction experiments on a single crystal provide evidence that the uranium moments align parallel to the *c* axis with the anisotropy energy of ≈ 170 K, indicating that U₂Ni₂Sn can be classified as an Ising system. The results are at variance with previous studies on polycrystals, which indicated different magnetic structure, and which were incompatible with the *5f* - *5f* two-ion anisotropy model dominant in most U band systems. High-field magnetization studies exhibit a weak linear response for fields along the basal plane up to the highest field applied (60 T), while the *c*-axis magnetization curve exhibits three metamagnetic transitions at approximately 30, 39, and 50 T. The U magnetic moments of $.87_{\mu\text{B}}$, the low magnetic entropy, and the enhanced Sommerfeld coefficient $\gamma = 187$ mJ/mol f.u. K² suggest that U₂Ni₂Sn can be classified as an itinerant antiferromagnet with strong electron-electron correlations.

I. INTRODUCTION

The uranium-based intermetallic compound U_2Ni_2Sn , which orders antiferromagnetically below $T_N = 25\text{--}26$ K, represents an important case for determining the underlying mechanism(s) of magnetic anisotropy in U intermetallics. Strong magnetic anisotropy, a vital ingredient for a variety of applications in permanent magnets or spintronic devices, is commonly associated with localized electronic states, that give rise to orbital magnetic moments, which couple the spin subsystem with particular preferred crystallographic directions. The microscopic mechanism, denoted as crystal electric field (CEF), is based on the spin-orbit interaction and the fact that states with different orbital-moment orientation have different charge distribution in real space, experiencing therefore different total energies in the presence of electrical field gradients. Typical examples are $4f$ metallic systems, where the interaction of the localized $4f$ states with the charge distribution around the $4f$ ion can be described as a single-ion effect. The lack of sizable orbital moments in lighter transition metals, such as Fe, Co, Ni, is the reason for anisotropy being negligibly small compared to the $4f$ systems. Stronger spin-orbit interaction in $5d$ systems cannot well manifest in anisotropy, as the broad $5d$ bands do not allow the formation of magnetic moments in bulk systems, but the situation can change in, e.g., mixed or artificial $3d\text{-}5d$ systems.

Unique opportunities are offered by actinides. For example, uranium systems give rise to ordered $5f$ magnetic moments, while enormous spin-orbit interaction leads inexorably to sizable orbital moments even if the $5f$ states are not localized [1]. The only precondition is the existence of spin moments. These can exist spontaneously in ferro- or antiferromagnets, but can also be induced by magnetic field in the paramagnetic state. In such systems the coupling of magnetic moments to the crystallographic directions is different. The $5f$ charge distribution is not the distribution of atomic-like wave functions as in the $4f$ materials, but is more dependent on bonding. The involvement of the states in bonding follows from the band character of the $5f$ states. The $5f$ localization takes place for heavier actinides (those beyond Pu, i.e., Am, Bk, Cf, etc.) and can occur even at U systems, although rarely, and is probably restricted to a few cases, such as UPd_3 [2].

Although details of electronic structure of individual materials can be quite intricate, the basic rules or tendencies of orbital-moments orientation should reflect the $5f\text{-}5f$ bonding

directions. The tendencies deduced theoretically for a hybridization-mediated anisotropy [3] were found indeed in real U-based intermetallics [4] with anisotropic U-U bonding. Magnetic anisotropy thus occurs in conjunction with elastic anisotropy [5].

While the conventional CEF effects vanish in dispersive, delocalized $5f$ electronic states of uranium, the directional $5f$ involvement in metallic bonding can be represented as preferential occupancy of the states with m_J perpendicular to the bonding directions. The $5f$ occupancy by two to three electrons per uranium guarantees that the situation is far from spherical symmetry. The anisotropy energy can be principally higher than in the CEF single-ion anisotropy. The attempt to rotate magnetic moments would have to lead to reconfiguration of the bonding situation, which is in many cases practically impossible, considering available magnetic fields of tens of teslas, producing Zeeman energies of a few meV only. As this type of anisotropy depends predominantly on the U-U coordination, it can be denoted as two-ion anisotropy.

Interesting attempts to quantify magnetic anisotropy by means of fully relativistic density functional theory (DFT) calculations with noncollinear orientations of U moments were undertaken for U_2Pd_2In , crystallizing in the same structure type as U_2Ni_2Sn [6]. High energies exceeding 8 mRy, i.e., 100 meV, were deduced as the difference between different orientations in the basal plane (where the moments lie in this compound). A large part of this can be denoted as anisotropy energy. A smaller part can be identified as being due to Dzyaloshinskii-Moriya exchange interactions. The calculations also revealed that almost antiparallel spin and orbit orientation remains in the course of the forced reorientation of the moments.

In parallel with *ab initio* calculations it is still important to see whether simple rules about U moments perpendicular to the U-U bonding directions are generally valid in diverse U systems. The magnetic anisotropy of several groups of U intermetallics with distinct type of U-U coordination indeed corresponds to the easy-magnetization direction perpendicular to the shortest U-U links, where the $5f$ bonding should be concentrated [4]. In particular, all compounds with dominant in-plane coordination revealed uniaxial anisotropy, while compounds with linear U chains have the chain axis as a hard magnetization direction. This rule was found so robust that it did not depend at all on the type of ligand atoms or the type of ground state (ferro, antiferro, paramagnetic). Importantly, the latter situation of U chains is relevant for unconventional

ferromagnetic superconductors UCoGe and URhGe [7], in which the magnetization can be reoriented by a field within the plane perpendicular to the chain axis, tuning magnetic fluctuations providing the coupling for superconductivity, but rotation to the chain axis is not possible.

The situation raised a question of what would happen if the variability of a particular structure type allows the changing of the types of nearest U-U neighbors. The few examples available suggest that the easy-magnetization direction may tend to follow such structure variations [5,8].

One of the structure types, which allows the observation of the impact of crossover of U-U distances, is the tetragonal structure Mo_2FeB_2 (SG $P4/mbm$), in which numerous $\text{U}_2\text{T}_2\text{X}$ compounds form for late transition metals T and X representing In, Sn, or a few other p -metals. This structure can be represented as a sequence of U and T - X sheets alternating along c ; however, the U-U spacing along the c axis is in most of cases shorter than the spacing within the basal plane. Moreover, there is only one nearest U neighbor in the basal plane at a distance not very different from the c -axis spacing. Hence, U atoms in the plane are coordinated in dimers, which can give rise to a system equivalent to the Shastry-Sutherland lattice, known as possible realization of the frustrated magnetic system. Therefore it is not surprising that U moments tend to orient perpendicular to c , as evidenced by neutron diffraction for $\text{U}_2\text{Pd}_2\text{In}$ and $\text{U}_2\text{Pd}_2\text{Sn}$ [9], or, e.g., $\text{U}_2\text{Ni}_2\text{In}$ [10]. The c -axis orientation of U moments is quite exceptional. It was found for $\text{U}_2\text{Rh}_2\text{Sn}$ [10,11], where the basal-plane neighbor distance 367.5 pm is somewhat longer than that of the two c -axis neighbors (362.4 pm), if we take data at $T = 30$ K [10]. This compound represents therefore an exception to the rule about orientation of U moments mentioned above. $\text{U}_2\text{Ni}_2\text{Sn}$ is, on the other hand, the only compound with the c -axis spacing much larger (369.3 pm) than the basal-plane spacing (357.5 pm) [12]. Consequently, U moments oriented along the c axis should be expected. The real orientation of the moments remained, however, a source of controversy.

First powder neutron-diffraction experiments revealed that the known antiferromagnetic order has a propagation vector $q = (0, 0, \frac{1}{2})$ and an antiferromagnetic (AF) coupling is also within the basal plane [12]. The orientation of moments was suggested to be in the basal plane, forming a collinear structure of the U moments ($\mu_{\text{U}} = 1.05 \mu_{\text{B}}$). However, from other possible models, the c -axis orientation gave only marginally worse fit. A most likely reason that Bourée et al. [12]

arrived at a magnetic moment in the basal plane is that for some of these tetragonal U_2T_2X -type compounds, such as U_2Ni_2Sn and U_2Rh_2Sn among others, the structure factors for several reflections including $(1, 0, \frac{1}{2})$, $(1, 1, \frac{1}{2})$, and $(2, 1, \frac{1}{2})$ which they primarily saw in their powder diffraction pattern, are very close in magnitude for both configurations of magnetic moments – within the basal plane and along the c axis – especially the $(1, 0, \frac{1}{2})$. This can be seen in the calculations published by both Pereira *et al.* and Nakotte *et al.* as shown in Refs. [11,10]. Therefore a refinement based on only a very few nonunique, with respect to intensities and structure factors along different configurations, has the potential to lead to inconclusive results. A single-crystal experiment was needed to resolve the case. Although some effort has been made to grow and study a single crystal, due to poor quality of the crystal, it has been difficult to report neutron diffraction data, allegedly pointing indeed to the c -axis orientation [13].

In the present work, we report successful synthesis of a U_2Ni_2Sn single crystal, which allowed us to determine the anisotropy of bulk properties as well as to draw a conclusion regarding the U-moments orientation from a neutron diffraction experiment. There exist extended experimental data on polycrystalline samples, describing basic magnetic and heat-capacity characteristics. An enhanced Sommerfeld coefficient $\gamma = 172$ mJ/mol f.u. K² was obtained for 1 mole based on two U atoms in the formula unit [14]. High magnetic fields applied at low temperatures induce a cascade of metamagnetic transitions with critical fields 30, 39, and 51 T [15]. The maximum field of 57 T still does not give any approach to saturation and the magnetization on free powder does not exceed $0.65 \mu_B/U$, i.e., much less than that predicted from powder neutron-diffraction data [12].

The negative resistivity slope $d\rho/dT$ in the paramagnetic state [16] is very different from experiments of other authors [17], which exhibit $d\rho/dT > 0$. Such disagreement may point to strongly anisotropic transport properties.

The direction of the U moments in the basal plane was determined for a deuteride of U_2Ni_2Sn , $U_2Ni_2SnD_{1.8}$, having a much higher Néel temperature, $T_N = 87$ K. This increase is most likely due to the volume expansion. The expansion is, however, strongly anisotropic and the shortest U-U links are in the c -axis direction in this case [18]. Existing *ab initio* calculations [19] do not address the issue of moment directions.

II. EXPERIMENTAL DETAILS

A single crystal was grown by the Czochralski method from an 8-g stoichiometric mixture of the pure elements (99.9% U, 99.99% Ni, and 99.9999% Sn) in a tri-arc furnace with a water-cooled copper crucible under protective argon atmosphere. A tungsten rod was used as a seed. The pulling speed was 10 mm/h. The phase purity and composition of the samples were checked by standard x-ray powder diffractometry and x-ray microanalysis. The backscattering x-ray Laue patterns showed the good quality of the crystals.

For a neutron-diffraction experiment, a cylindrical single crystal of $\text{U}_2\text{Ni}_2\text{Sn}$ with an approximate volume of 2 mm^3 was extracted from the ingot. The temperature dependence of the lattice parameters was measured by x-ray powder diffraction (XRD) using Co radiation and by a single-crystal neutron diffraction (ND) experiment performed on the Single Crystal Diffractometer (SCD) at the Los Alamos Neutron Science Center, LANL, NM, USA. The refinements of the XRD and ND were carried out using the FULLPROF suite package [20] and GSAS [21], respectively.

The magnetic susceptibility was measured along the principal crystallographic directions using a SQUID magnetometer in the temperature range 2–300 K and magnetic fields up to 7 T. The measurement of magnetization was extended to 60 T using the pulsed-field magnet of the high-field facility at Rossendorf, Germany, using a nondestructive pulsed-field magnet with pulse duration of 25 ms. The magnetization signal was detected by an induction method with a standard pick-up coil system [22]. For the magnetoacoustic measurements, two piezoelectric film transducers were glued onto parallel polished facets of the single crystal and the measurements were performed using a pulse-echo technique [23]. The propagation vector k and polarization vector u were directed along the a axis; the ultrasound frequency was 72 MHz. The specific heat was measured on a single crystal by means of a Quantum Design PPMS in the temperature range 2–300 K.

Additional magnetic neutron-diffraction experiments were performed at the HB3A four-circle diffractometer at the High Flux Isotope Reactor, ORNL, USA. The neutron wavelength of 1.546 \AA was used from a bent perfect Si-220 monochromator [24]. Further details are given in the section describing experimental data.

III. RESULTS AND DISCUSSION

A. Crystal structure

Laue x-ray diffraction performed on a $\text{U}_2\text{Ni}_2\text{Sn}$ single crystal revealed a single grain adopting a tetragonal structure (see Fig. 1). The Laue patterns were taken at various places on the crystal including the reversion of the crystal by 180° between two successive measurements.

Table I. Room-temperature structural parameters of $\text{U}_2\text{Ni}_2\text{Sn}$ obtained from the x-ray diffraction analysis.

Lattice parameters: $a = 7.267(3) \text{ \AA}$, $c = 3.691(2) \text{ \AA}$					
Atom	Position	x	y	z	Occupancy
U	$4h$	0.1757(1)	0.6757(1)	0.5	1
Ni	$4g$	0.6234(1)	0.1234(1)	0	1
Sn	$2a$	0	0	0	1

The crystal structure of $\text{U}_2\text{Ni}_2\text{Sn}$ was studied at room temperature by x-ray powder diffraction. The x-ray reflections were indexed in the space group $P4/mbm$. The room-temperature structural parameters of $\text{U}_2\text{Ni}_2\text{Sn}$ are given in Table I. The lattice parameters a and c are close to those reported by other groups ($a = 7.2690 \text{ \AA}$, $c = 3.6929 \text{ \AA}$ [12], $a = 7.261 \text{ \AA}$, $c = 3.694 \text{ \AA}$ [23]).

Single-crystal neutron-diffraction data were collected at various temperatures. The neutron-diffraction patterns were indexed in tetragonal symmetry with space group $P4/mbm$. The structural parameters of $\text{U}_2\text{Ni}_2\text{Sn}$ at various temperatures were determined using GSAS, and these were taken to compute the shortest interatomic distances. The temperature dependencies of the shortest interatomic distances for $\text{U}_2\text{Ni}_2\text{Sn}$ are listed in Table II.

For $\text{U}_2\text{Ni}_2\text{Sn}$, the shortest U-U links perpendicular to the c axis ($d^\perp_{\text{U-U}}$) are considerably shorter than the corresponding shortest U-U links along the c axis. Contrary to expectations from usual thermal-expansion behavior, the $d^\perp_{\text{U-U}}$ increases with decreasing temperature, while $d^\parallel_{\text{U-U}}$ decreases with decreasing temperature.

The results of the neutron-diffraction experiment are corroborated by the x-ray powder diffraction. It confirms that the a parameter increases with increasing temperature while the c parameter decreases (Fig. 2, left). Any spontaneous magnetostriction effect, i.e., additional change of a and c in the ordered state, is below the resolution of present experiment. The shortest U-U distance at all temperatures is found to be in the basal plane, although it increases with increasing temperature (Fig. 2, right). A similar temperature dependence was found also for $\text{U}_2\text{Pd}_2\text{Sn}$ [9]. In $\text{U}_2\text{Ni}_2\text{Sn}$ the shortest inter-uranium distance has a similar temperature dependence as the lattice parameter a . The temperature dependence of the U position manifests itself at low temperatures (below T_N) where the $d_{\text{U-U}}$ in the basal plane increases relatively by 4×10^{-3} . As shown in Fig. 3, the internal parameters x and y of the U position, which determine the inclination of the basic square motif, can have an impact on $d_{\text{U-U}}^{\perp}$.

Table II. Shortest interatomic distances in $\text{U}_2\text{Ni}_2\text{Sn}$, $d_{\text{U-U}}^{\parallel}$ (parallel to the c axis), $d_{\text{U-U}}^{\perp}$ (perpendicular to the c axis), $d_{\text{U-Ni}}$, and $d_{\text{U-Sn}}$ obtained from the neutron-diffraction analysis.

T (K)	$d_{\text{U-U}}^{\parallel}$ (Å)	$d_{\text{U-U}}^{\perp}$ (Å)	$d_{\text{U-Ni}}$ (Å)	$d_{\text{U-Sn}}$ (Å)
300	3.680(2)	3.579(2)	2.757(2)	3.246(3)
180	3.683(1)	3.574(1)	2.754(1)	3.245(3)
130	3.688(1)	3.567(1)	2.756(1)	3.244(3)
80	3.694(2)	3.560(1)	2.754(1)	3.242(3)
40	3.700(1)	3.555(1)	2.753(1)	3.234(3)

B. Magnetization measurements

The temperature dependence of magnetic susceptibility, $\chi(T)$, was measured with magnetic field applied along the c axis and in two directions in the basal plane using a SQUID magnetometer (Fig. 4). The susceptibility values along c were found higher in the whole temperature range; the susceptibilities along $[100]$ and $[110]$ are identical. In the paramagnetic state, the data were fitted to the Curie-Weisslaw, yielding the paramagnetic Curie temperatures $\theta_{\text{p}[110]} = -248$ K and $\theta_{\text{p}[001]} = -75$ K, while the effective magnetic moment $\mu_{\text{eff}} = 3.8 \mu_{\text{B}}/\text{mol f.u.}$ ($2.7 \mu_{\text{B}}/\text{U}$) is independent of the direction. The difference of the θ_{p} values, $\Delta\theta_{\text{p}} \approx 170\text{K}$, gives an estimate of the magnetic

anisotropy energy per U atom, $E_a = \Delta\theta_p k_B = 14.6$ meV or, alternatively, an anisotropy field $\mu_0 H_a = 285$ T for the $0.87 \mu_B$ moment, derived from the neutron diffraction below.

The transition to the antiferromagnetic state appears as an anomaly at $T = 25$ K, which agrees with the value indicated for polycrystalline samples [14,25]. Furthermore, the absolute values of susceptibility averaged over all directions correspond well to those obtained on a crushed polycrystal with randomly oriented grains [14]. The comparison of single-crystal and polycrystal, however, illustrates the clear fact that the averaging leads to a bending of $1/x$ vs T , which has to be accommodated by additional temperature-independent term x_0 , and the μ_{eff} values on the polycrystal come out smaller ($2.3 \mu_B/U$ in this case [14]). One can notice that the shape of the T_N anomaly is different for different field orientations. While a sharp cusp was observed at T_N for the field within the basal plane, the c -axis orientation exhibits a gradual deviation from CW behavior and $x(T)$ forms a broad rounded maximum at 30–32 K. The actual T_N manifests as a precipitous drop. One can speculate that the different critical behavior is due to antiferromagnetic correlations, i.e., intersite effect, with possible different correlation lengths along various directions, or local spin fluctuations as an effect of destabilization of the individual moments above T_N [26].

In magnetic fields on the scale of several teslas, the susceptibility (M/H) was found to be field independent. For the field along the basal plane, it is true also to very high fields. This can be seen from the linear dependence $M(H)$ in Fig. 5. This would mean that the three metamagnetic transitions, at about 30, 39, and 50 T, observed in [15] take place exclusively with the field along c . Indeed, it is the case. The transitions have only somewhat sharper contours than for the field-aligned powder sample, used in Ref. [15]. Also the magnetization of $1.3 \mu_B/\text{f.u.}$ in $\mu_0 H = 57$ T [15] for polycrystal is only slightly smaller than that of the well-oriented single crystal, reaching $1.4 \mu_B/\text{f.u.}$ in the same field. All transitions are practically reversible. The observed hysteresis in the transitions at $T = 1.5$ K does not exceed 0.1 T and vanishes fast with increasing T . Measurements at elevated temperatures reveal that the shift of the critical fields to lower values, expected in antiferromagnets, is very small.

C. Specific-heat measurement

Zero-field specific heat C_p shows a sharp λ -type anomaly with a maximum at 25.1 K, corresponding to the magnetic phase transition (Fig. 6). The low-temperature part can be well

approximated by a $C_p = \gamma T + \beta T^3$ dependence (not shown here). The linearity extends to almost 20 K, which clearly indicates the absence of spin wave excitations. Indeed, such Ising-like behavior is expected at temperatures far below the uniaxial anisotropy energy. Because a slight nonlinearity appears below 50 K, we performed fitting in the range 50–300 K, which gives a Sommerfeld coefficient of the electronic specific heat $\gamma = 187$ mJ/mol f.u.K². This value is somewhat higher than $\gamma = 172$ mJ/mol f.u.K², as determined for a polycrystal [14]. The coefficient $\beta = 2.09$ mJ/mol f.u.K⁴ gives a Debye temperature $\Theta_D = 167$ K which agrees well with the value $\Theta_D = 168$ K determined for the isostructural compound U₂Rh₂Sn in the ordered state [27].

The analysis of the specific heat in the whole temperature range studied (Fig. 7) indicates that the paramagnetic range can be well described by a standard Debye model using the Debye temperature $\Theta_D = 207$ K, i.e., somewhat higher than 167 K estimated from the low-temperature slope of $C_p/T(T^2)$. This disagreement indicates that the crystal lattice is stiffer in the paramagnetic state. The Sommerfeld coefficient in the paramagnetic state can be deduced as 90 mJ/mol f.u.K². In conventional antiferromagnets, the γ value in the ordered state can be lower than the paramagnetic value in case the Fermi surface is affected by a superzone gapping by additional periodicity in an antiferromagnet. In our case, we observe an opposite tendency, which points to a significant many-body enhancement at low temperatures.

Using the Debye function as a background for estimating the magnetic entropy (obtained as the integral of the area between experimental C_p/T values and the nonmagnetic background), we see that, although the magnetic entropy still increases to about 50 K, it does not reach the value $R \ln 2$, the expected entropy difference between ordered and paramagnetic states for a doublet, with moment only up or down (Fig. 8). A slightly lower estimate of the magnetic entropy is obtained if the low-temperature $\gamma = 187$ mJ/mol f.u.K² is used. The result, shown as the red line in Fig. 8, gives about 50% of $R \ln 2$ up to T_N . The fact that the magnetic entropy continues to increase up to $T = 50$ K can be attributed mainly to a short-range order above T_N . The difference between the experimental data and the red line is to a large extent due to the difference in the lower Debye temperature in the ordered state and higher value used to the red line. (It corresponds to a low-temperature γ value but Θ_D is that of the paramagnetic state). The reason is that no low-lying magnetic excitations are expected in an Ising system with T_N much lower than the anisotropy energy (170 K). Hence the real magnetic entropy can be even smaller than the values displayed in

Fig. 8. Using the low- T γ as well as $\Theta_D = 167$ K (not shown here) gives the dependence retracing the experimental data up to $T = 20$ K, which would mean that no magnetic excitations are significant for specific heat up to this temperature. In the range 20–25 K, the experimental data increase over the Debye dependence, but the integrated entropy is on the level of $0.01R \ln 2$.

D. Magnetoacoustic properties

Relative sound-velocity changes, $\Delta v/v$, show hardening with decreasing temperature (Fig. 9). The phase transition at 25 K leads to a change of slope of the $\Delta v/v(T)$ dependence. In the magnetically ordered state, additional hardening is observed. Altogether, the sound velocity increases by 0.2% below T_N . The hardening seems to be in contradiction with estimated lower Debye temperature in the ordered state. However, while the acoustic effects were measured for the a axis only, the scalar Θ_D parameter reflects all lattice directions.

All three metamagnetic transitions are accompanied by pronounced anomalies in the acoustic characteristics. Figure 10 shows magnetoacoustic effects at $T = 1.5$ K. Although the transitions in the magnetization curves look similar, the acoustic anomalies are rather different. The first transition at $\mu_0 H_{cr1} = 30$ T (which is practically temperature independent and present up to T_N) produces a step down in the sound velocity and is not seen at all in the sound attenuation, $\Delta\alpha$. The second (at $\mu_0 H_{cr2} = 40$ T and also temperature independent) and third ($\mu_0 H_{cr3} = 52$ T at 1.5 K and decreasing with increasing temperature) transitions exhibit a deep minimum in sound velocity and an anomaly in attenuation. Both effects are especially large at the second transition. Moreover, their temperature evolution is strongly nonmonotonous (Figs. 11 and 12). Depth of the minimum in sound velocity $\Delta v/v$ starts from 2×10^{-3} at 1.5 K, passes through maximum value 22×10^{-3} at 12 K, and then vanishes approaching T_N . Similarly, the peak in sound attenuation is 4 dB/cm (1.5 K), 60 dB/cm (12 K), and 2 dB/cm at 20 K. Enhanced attenuation at H_{cr2} indicates that the first-order transition (which has phase separation but not critical fluctuations) changes at elevated temperatures into second order with diverging critical fluctuations. May speculate that the culmination of the parameters for the middle transition at 12 K may be associated with a tricritical point, in which the first-order transition at lower temperatures changes into the second-order type. In such situation the potential barrier between two different configurations of magnetic

moments vanishes; i.e., the phase coexistence combines with zero latent heat or hysteresis, which promotes massive fluctuations leading to large attenuation and lattice softening.

The sharp anomalies in $\Delta v/v$ and $\Delta\alpha$ at the second transition provide a way to estimate a characteristic relaxation time of fluctuations of magnetic moments at this transition. Our data can be interpreted using a Landau-Khalatnikov-type formula [28],

$$\alpha = -\frac{\Delta C \omega^2 \tau}{c \cdot 2v}, \quad (1)$$

where C is elastic modulus, ω is angular frequency, and τ is relaxation time. Equation (1) is valid in the limit $\omega\tau \ll 1$. We approximated relative elastic-modulus changes, $\frac{\Delta C}{C}$, using the relation, $\frac{\Delta C}{C} = 2\frac{\Delta v}{v}$. From Eq. (1), we obtain $\tau \approx 10^{-9}$ s between 2 and 20 K. Although this relaxation time of moments is larger than typical electronic collision times, $\omega\tau$ is still much smaller than 1.

We have no direct information on the magnetic structure in high magnetic fields. As to the structure of the ground state, we refer to the next section, where a plausible model based on collinear AF structure with magnetic unit cell doubled along the c axis is proposed. The individual increments of magnetization at the metamagnetic transition are very small. Considering the magnetic unit cell consisting of four spin-up and four spin-down moments, a simple flip of one moment would give an increment of one-quarter of the size of the U moment, i.e., more than $0.2 \mu_B$ considering the $0.87 \mu_B/U$ moments deduced below. On the other hand, it is known (see, e.g., Ref. [29]) that a simple Ising system with two different exchange parameters for different types of neighbors can yield a very complicated sequence of phases, called a devil's staircase. The high anisotropy is, however, a determining factor, which should give a strong preference to collinear structures with moments along c even in high magnetic fields. Hence all metamagnetic transitions should be of the spin-flip type.

Table III. Observed magnetic intensities of U_2Ni_2Sn and calculated intensities by fitting to a magnetic structure with magnetic moment of uranium atoms along the c axis.

h	k	l	$I(\text{obs})$	σ	q^2	$ F_{hkl} ^2$	$I(\text{calc})$
0	0	0.5	0.00	0.14	0.0005	0.0	0.00
1	0	0.5	2.91	0.27	0.0009	3.29	2.67

3	0	0.5	15.83	0.72	0.0048	15.61	14.79
1	1	0.5	10.21	0.41	0.0014	10.08	10.32
2	1	0.5	1.08	0.14	0.0029	1.14	1.19
3	1	0.5	0.00	0.27	0.0053	0.31	0.28
3	2	0.5	4.27	0.36	0.0067	5.39	4.13
4	2	0.5	5.96	0.35	0.0101	9.47	5.28
3	0	1.5	5.62	0.29	0.0085	15.61	5.13
1	1	1.5	2.02	0.17	0.0051	10.08	1.84
2	1	1.5	0.54	0.37	0.0066	1.14	0.34
2	2	1.5	1.01	0.43	0.0080	6.85	2.32
3	2	1.5	2.01	0.31	0.0104	5.39	1.74

E. Magnetic structure studied by neutron diffraction

The low-temperature neutron-diffraction experiment at ORNL, USA, was performed in order to determine the magnetic structure. The four-circle diffractometer HB3A at the High Flux Isotope Reactor equipped with a closed-cycle He displacer was used. A neutron beam of the wavelength of 1.546 Å was provided by a PG(002) monochromator. A pyrolytic graphite filter was inserted in the neutron beam path in front of the sample to reduce the $\lambda/2$ contamination. The diffraction peaks were fitted to Gaussians and the integrated intensities were corrected for the Lorentz and extinction factor. The data for magnetic-structure determination were collected at $T = 5\text{K}$ using intensities of all magnetic Bragg reflections up to $\sin \theta/\lambda = 0.32\text{\AA}^{-1}$. Observed and calculated reflections with $I > 3\sigma$ are listed in the Table III. The nuclear peaks closest to the magnetic ones were used to apply corrections to the magnetic peaks. The extinction parameter was refined during the fitting of the intensities for the magnetic structure models. The magnetic-structure models were determined by the BASIREPS program within the FULLPROF suite package and the basis vectors were determined using the same [24].

Following the analysis of possible magnetic structures in Ref. [12], we assume that the U magnetic moments are either along the c axis or within the basal plane, along the mirror planes of the $[110]$ type or perpendicular to them. Our data indicate a clear preference for the Γ_8 type of structure, which is a collinear antiferromagnetic structure with c -axis direction of the U moments with alternating orientation within each unit cell and propagation vector $k = (0, 0, \frac{1}{2})$, which is equivalent to that of $\text{U}_2\text{Rh}_2\text{Sn}$ [11]. The refined U moment, $0.87 \mu_{\text{B}}$, is, however, higher than for $\text{U}_2\text{Rh}_2\text{Sn}$ ($0.53 \mu_{\text{B}}/\text{U}$). The weighted χ^2 is 2.45 and the refined extinction parameter [24] is 5.20.

Our attempts to fit the observed intensities to a $I 10$ type structure yielded unacceptably poor fits with χ^2 values above 0. No Ni moments were considered. It is interesting to point out that the U magnetic moment in $\text{U}_2\text{Ni}_2\text{Sn}$ is very close to the value obtained for the deuteride [$0.8(3) \mu_{\text{B}}$], which has, however, different magnetic structure [18]. The magnetic structure of $\text{U}_2\text{Ni}_2\text{Sn}$ is shown in Fig. 1 (right).

The temperature dependence of the $(11 \frac{1}{2})$ peak was measured in the range 5–35 K. As shown in Fig. 13, the decrease of the intensity with increasing T can be well accounted for by the expression $I = I_0(1-T/T_C)^{2\beta}$ with the critical exponent $\beta = 0.20$, which is somewhat lower than $\beta = 0.28$ for $\text{U}_2\text{Rh}_2\text{Sn}$ [11]. This value is not only lower than the mean field $\beta = 0.5$ or Heisenberg-like 0.38 (for $S = 1/2$), but also lower than the three-dimensional (3D) Ising value $5/16 \approx 0.31$ and approaching the two-dimensional (2D) Ising value $\beta = 1/8 = 0.125$ [30]. This fact can be probably attributed to anisotropic interactions in the Ising system. The fit indicates that the magnetic moment at $T = 5$ K can be by 4.7% lower than the limit one at $T = 0$ K, which then would be $0.92 \mu_{\text{B}}/\text{U}$. The fit using only data from 22–26 K gives $\beta = 0.30$ with a transition temperature of 26.3 K. This value of β is closer to the value for three-dimensional systems.

F. Discussion

The single-crystal study of the anisotropy and magnetic structure of $\text{U}_2\text{Ni}_2\text{Sn}$ demonstrates that this compound does not contradict general tendencies locating the easy magnetization direction, which is the c axis, perpendicular to the shortest U-U bonds. The antiferromagnetic propagation vector $q = (0, 0, \frac{1}{2})$ and the type of coupling of four U moments within the unit cell confirmed the initial report [12], but the reported moments orientation within the basal plane (without single preferred direction) has flipped into the unique tetragonal axis. The magnetic structure of $\text{U}_2\text{Ni}_2\text{Sn}$ is hence identical to that found in [31] for $\text{U}_2\text{Ni}_2\text{Sn}$ with Ni substituted by 30% Pd.

The flipping of the easy-magnetization direction within one crystal-structure type, following (with very few exceptions) the crossover of the U-U spacings, is a quite remarkable fact, confirming the dominant role of the two-ion bonding anisotropy. Other influences, such as the Dzyaloshinskii-Moriya interaction, do not clearly play a decisive role.

Table IV. Summary of U-moment orientations, types of the U-U coordination ($d_{U-U}^{\parallel}/d_{U-U}^{\perp} < 1$ indicates the shortest U-U distance along the c axis), and type of magnetic interactions between nearest U neighbors d_{1U} , d_{2U} , d_{4U} (the number of such neighbors, n , is indicated by the digit in the index of d_{nU}). The table captures both the structure parameters at room temperature (RT) and in the ordered state at low temperatures.

	$d_{U-U}^{\parallel}/d_{U-U}^{\perp}$	$\mu_U(\mu_B)$	μ_U Orientation	Reference	$d_{1U}(\perp c)$	$d_{4U}(\perp c)$	$d_{2U}(\parallel c)$
U ₂ Ni ₂ Sn	1.028 (RT)	0.87	c axis	This paper	F	AF	AF
	1.046 (5 K)						
U ₂ Ni ₂ SnD _{1.8}	1.000 (120 K)	0.8	Basal plane	[18]	AF	$\pi/2$	F
U ₂ Rh ₂ Sn	0.980 (RT)	0.38	c axis	[10,27]	F	AF	AF
	0.990 (8 K)						
U ₂ Pd ₂ In	0.941 (RT)	1.6	Basal plane	[9]	AF	$\pi/2$	F
U ₂ Pd ₂ Sn	1.002 (RT)	2.0	Basal plane	[9]	AF	$\pi/2$	F
	0.994 (10 K)						
U ₂ Ni ₂ In	0.992 (RT)	0.60	Basal plane	[10]	AF	$\pi/2$	AF

U₂Ni₂Sn belongs to the magnetically ordered U₂T₂X compounds. The order appears for the last d elements of a series, which indicates that the $5f$ - d hybridization, being weak in such a situation, is responsible for the loss of magnetic order for less-filled d states. However, even for the last transition metals the $5f$ localization cannot be achieved, which is demonstrated by the low ordered moments and the very low magnetic entropy of U₂Ni₂Sn. From other compounds, U₂Rh₂Sn is rather similar, exhibiting the same type of anisotropy as well as magnetic structure and almost identical $T_N = 25$ K.

For the latter compound, it is more difficult to quantify the anisotropy in a similar way as for U₂Ni₂Sn, where simply the difference in paramagnetic Curie temperatures can be taken as a measure of the energy, provided that all directions exhibit the same effective-moment value. However, the data for U₂Rh₂Sn [27] yield different effective moments for the field along the a and c axes. The $1/\chi(T)$ dependencies were obtained not as linear, but bent, which was accounted for in the fitting by different values of temperature-independent term χ_0 . The bending of $1/\chi(T)$ in the paramagnetic range may be, for example, also a sign of mosaicity of the single crystal used or its slight misorientation, both distorting the message quantifying the anisotropy. Interesting insight

may be provided by experiments with, e.g., Fe substitution for Ni, which should give the two shortest U-U spacings approaching each other [32].

Table IV reviews the relation of the U-moments orientation and the U-U coordination, expressed as the ratio $d_{U-U}^{\parallel}/d_{U-U}^{\perp}$ for U_2Ni_2Sn , and U_2Rh_2Sn and selected other U_2T_2X compounds. It is evident that U_2Rh_2Sn with $d_{U-U}^{\parallel}/d_{U-U}^{\perp} = 0.998$ is the only exception; otherwise $d_{U-U}^{\parallel}/d_{U-U}^{\perp} > 1$ implies the c -axis orientation, and $d_{U-U}^{\parallel}/d_{U-U}^{\perp} < 1$ the basal-plane orientation, confirming the predominant influence of the shortest U-U distances forcing the U moments perpendicular to them. In addition, the overview indicates a strong tendency for the ferromagnetic coupling between nearest U atoms, whether they are along c (d_{2U}) or within the basal plane (d_{1U}). This fact corroborates the relevance of the two-ion anisotropy model, assuming the strong ferromagnetic coupling along the strong-bonding axis [3].

Multiple metamagnetic transitions with relatively small magnetization steps are reminiscent of the behavior of Shastry-Sutherland magnets, of which some (e.g., rare-earth tetraborides) exhibit the same coordination of the f atoms [33]. However, the type of magnetic structure realized (at least in zero field) is not frustrated. The ferromagnetic coupling in the short Shastry-Sutherland bonds, i.e., between the nearest U moments (within the basal-plane unit cell across the unit cell boundary) is compatible with the AF coupling between the moments within the unit cell, which are more far away. The behavior in high magnetic fields can be, however, different and frustration can be expected, as found for TmB_4 with fractional magnetization steps [33]. The complex magnetic phase diagram (see Fig. 14), constructed from the magnetization and magnetoacoustic data, shows the possibility of interesting magnetization states. High magnetic fields (when compared to TmB_4) needed to modify the magnetic structure can be attributed to a strong AF exchange between the next-nearest neighbors within the basal plane as well as to AF exchange along the c axis. In actinides, a rich sequence of field induced magnetic phases can appear even in materials with simple lattice geometry, as UAs [34], so the frustration need not be necessary. On the other hand, isostructural regular rare-earth compounds (RE_2T_2X) may exhibit complicated metamagnetism. An example is Tb_2Pd_2In [35], but more systematic information on single crystals is so far lacking. From anomalous rare earths, a rich sequence of metamagnetic transitions, observed for Yb_2Pt_2Pb [36] could be interpreted in terms of the Shastry-Sutherland frustration.

IV. CONCLUSIONS

Although earlier reports indicated a basal-plane orientation of U moments in U_2Ni_2Sn , the single-crystal studies yield their c -axis orientation both from neutron-diffraction and bulk magnetization measurements, proving the c axis to be the easy-magnetization direction. The compound therefore does not contradict prediction of the two-ion anisotropy model, requesting the moments perpendicular to the shortest U-U links. Exceptional structure geometry of U_2Ni_2Sn , having the U-U links in the basal plane shorter than the c -axis U-U distances by a large margin, therefore allows us to prove that the U moments flip indeed with respect to most of other U_2T_2X compounds, where the c -axis spacing is the shortest.

The enhanced Sommerfeld coefficient γ , low magnetic entropy, and ordered and effective moments far below free-ion predictions ($\mu_{\text{eff}} = 3.6 \mu_B/U$ is expected for free U ion) evidence the band character of the $5f$ states. However, the reduced $5f$ - $3d$ hybridization in the case of Ni with almost-filled $3d$ states allows the use of the local-moment picture, with Curie-Weiss behavior of paramagnetic susceptibility with the same μ_{eff} value, $2.7\mu_B/U$, irrespective of the field direction. The difference in respective paramagnetic Curie temperatures of 170 K allows the quantification of the magnetic anisotropy energy, reaching almost 15 meV/U atom. Hence it is quite understandable that only a weak linear response of magnetization is recorded for the field along the basal plane. Despite very high fields applied (60 T), no sign of moment reorientation has been found. Applying the same field along the easy axis, a cascade of metamagnetic transitions with relatively small magnetization increments has been found, which suggests a complicated development of magnetic structures in such high magnetic fields.

ACKNOWLEDGMENTS

This work was supported by the Czech Science Foundation under Grants No. 18-02344S and No. 16-03593S. Neutron scattering studies were performed at the Los Alamos Neutron Science Center (LANSCE) and Oak Ridge High Flux Isotope Reactor (HFIR), both DOE Office of Science User Facilities. We acknowledge the support of the High Magnetic Field Laboratory (HLD) at Helmholtz-Zentrum Dresden-Rossendorf (HZDR), a member of the European Magnetic Field Laboratory (EMFL). The authors are indebted to Frank de Boer for careful reading of the manuscript.

REFERENCES

- [1] M. S. S. Brooks and P. J. Kelly, Large Orbital-Moment Contribution to $5f$ Band Magnetism, *Phys. Rev. Lett.* 51, 1708 (1983).
- [2] Y. Baer and H. R. Ott, $5f$ electron localization in intermetallic UPd₃, *Solid State Commun.* 36, 387 (1980).
- [3] B. R. Cooper, R. Siemann, D. Yang, P. Thayamballi, and A. Banerjea, *Handbook of the Physics and Chemistry of the Actinides*, edited by A. J. Freeman and G. H. Lander (North-Holland, Amsterdam, 1985), Vol. 2, Chap. 6, p. 435.
- [4] L. Havela, V. Sechovský, F. R. de Boer, E. Brück, and H. Nakotte, Magnetic anisotropy in UTX compounds, *Phys. B (Amsterdam, Neth.)* 177, 159 (1992).
- [5] S. Mašková, A. M. Adamska, L. Havela, N.-T. H. Kim-Ngan, J. Przewoźnik, S. Daniš, K. Kothapalli, A. V. Kolomiets, S. Heathman, H. Nakotte, and H. Bordallo, Lattice anisotropy in uranium ternary compounds: UTX, *J. Alloys Compd.* 522, 130 (2012).
- [6] L. M. Sandratskii, Dzyaloshinskii-Moriya and magnetic anisotropies in uranium compounds, *Phys. B (Amsterdam, Neth.)* 536, 512 (2018).
- [7] D. Aoki and J. Flouquet, Ferromagnetism and superconductivity in uranium compounds, *J. Phys. Soc. Jpn.* 81, 011003 (2012).
- [8] L. Havela, S. Maskova, A. Adamska, A. V. Kolomiets, N. T.-H. Kim-Ngan, S. Danis, S. Heathman, K. Kothapalli, H. Nakotte, and H. Bordallo, Lattice and magnetic anisotropies in uranium intermetallic compounds, *Solid State Phenomena* 194, 75 (2013).
- [9] A. Purwanto, R. A. Robinson, L. Havela, V. Sechovsky, P. Svoboda, H. Nakotte, K. Prokes, F. R. de Boer, A. Seret, J. M. Winand, J. Rebizant, and J. C. Spirlet, Magnetic Ordering in U₂Pd₂In and U₂Pd₂Sn, *Phys. Rev. B* 50, 6792 (1994).

- [10] H. Nakotte, A. Purwanto, R. A. Robinson, L. Havela, V. Sechovsky, L. J. C. Pereira, A. Seret, J. Rebizant, J. C. Spirlet, and F. Trouw, Hybridization Effects in U_2T_2X Compounds: Magnetic Structures of U_2Rh_2Sn and U_2Ni_2In , *Phys. Rev. B* **53**, 3263 (1996).
- [11] L. C. J. Pereira, J. A. Paixão, P. Estrela, M. Godinho, F. Bourdarot, M. Bonnet, J. Rebizant, J. C. Spirlet, and M. Almeida, A single-crystal magnetization and neutron scattering investigation of the magnetic structure of U_2Rh_2Sn , *J. Phys.: Condens. Matter* **8**, 11167 (1996).
- [12] F. Bourée, B. Chevalier, L. Fournès, F. Mirambet, T. Roisnel, V. H. Tran, and Z. Zolnierek, Crystal and magnetic structures of U_2Ni_2Sn investigated by neutron diffraction and ^{119}Sn Mössbauer spectroscopy, *J. Magn. Magn. Mater.* **138**, 307 (1994). [13] D. Laffargue, B. Chevalier, S. F. Matar, and F. Bourée (private communication).
- [14] L. Havela, V. Sechovský, P. Svoboda, H. Nakotte, K. Prokeš, F. R. de Boer, A. Seret, J. M. Winand, J. Rebizant, J. C. Spirlet, A. Purwanto, and R. A. Robinson, Magnetism in U_2T_2X compounds, *J. Magn. Magn. Mater.* **140–144**, 1367 (1995).
- [15] T. Fukushima, S. Matsuyama, T. Kumada, K. Kindo, K. Prokes, H. Nakotte, F. R. de Boer, L. Havela, V. Sechovsky, J. M. Winand, J. Rebizant, and J. C. Spirlet, High-field magnetization studies of some U_2T_2X compounds, *Phys. B (Amsterdam, Neth.)* **211**, 142 (1995).
- [16] K. Kindo, T. Fukushima, T. Kumada, F. R. de Boer, H. Nakotte, K. Prokeš, L. Havela, V. Sechovský, A. Seret, J. M. Winand, J. C. Spirlet, and J. Rebizant, Electronic properties of U_2Ni_2Sn , *J. Magn. Magn. Mater.* **140–144**, 1369 (1995).
- [17] R. P. Pinto, M. M. Amado, M. A. Salgueiro, M. E. Braga, J. B. Sousa, B. Chevalier, F. Mirambet, and J. Etourneau, Transport and magnetic properties of U_2Ni_2Sn and U_2Co_2Sn , *J. Magn. Magn. Mater.* **140–144**, 1371 (1995).
- [18] K. Miliyanchuk, L. Havela, L. C. J. Pereira, A. P. Gonçalves, and K. Prokeš, Peculiarities of U_2T_2X hydrides, *J. Magn. Magn. Mater.* **310**, 945 (2007).
- [19] S. F. Matar and A. F. Al Alam, First principles study of the electronic and magnetic structure of $U_2Ni_2SnH_2$, *New J. Phys.* **10**, 083013 (2008).

- [20] J. Rodriguez-Carvajal, Recent developments of the program FULLPROF, Comm. Powder Diffr. IUCr Newsl. **26**, 12 (2001).
- [21] A. C. Larson and R. B. Von Dreele, General Structure Analysis System (GSAS), Los Alamos National Laboratory Report No. LAUR 86-748, 2000 (unpublished).
- [22] Y. Skourski, M. D. Kuźmin, K. P. Skokov, A. V. Andreev, and J. Wosnitza, High-field magnetization of $\text{Ho}_2\text{Fe}_{17}$, Phys. Rev. B **83**, 214420 (2011).
- [23] B. Wolf, B. Lüthi, S. Schmidt, H. Schwenk, M. Sieling, S. Zherlitsyn, and I. Kouroudis, New experimental techniques for pulsed magnetic fields—ESR and ultrasonic, Phys. B (Amsterdam, Neth.) **294–295**, 612 (2001).
- [24] B. C. Chakoumakos, H. B. Cao, F. Ye, A. D. Stoica, M. Popovici, M. Sundaram, W. Zhou, J. S. Hicks, G. W. Lynn, and R. A. Riedel, J. Appl. Crystallogr. **44**, 655 (2011).
- [25] F. Mirambet, B. Chevalier, L. Fournès, P. Gravereau, and J. Etourneau, Investigation of ^{119}Sn Mössbauer spectroscopy, magnetic and electrical resistivity measurements of $\text{U}_2\text{M}_2\text{Sn}$ stannides ($M = \text{Fe}, \text{Co}, \text{Ni}, \text{Ru}, \text{Rh}, \text{Pd}$), J. Alloys Compd. **203**, 29 (1994).
- [26] G.-J. Hu, N. Kioussis, and B. R. Cooper, Resonant band- f scattering and the magnetic properties of highly correlated actinide systems, J. Appl. Phys. **61**, 3385 (1987).
- [27] K. Prokes, D. I. Gorbunov, M. Reehuis, B. Klemke, A. Gukasov, K. Uhlirova, X. Fabrèges, Y. Skourski, F. Yokaichiya, S. Hartwig, and A. V. Andreev, Anisotropic physical properties of single-crystal $\text{U}_2\text{Rh}_2\text{Sn}$ in high magnetic fields, Phys. Rev. B **95**, 174433 (2017).
- [28] L. D. Landau and E. M. Lifshitz, *Fluid Mechanics* (Addison-Wesley, Boston, 1959), p. 304.
- [29] P. Bak and J. von Boehm, Ising model with solitons, phasons, and “the devil’s staircase”, Phys. Rev. B **21**, 5297 (1980).
- [30] M. E. Fisher, The theory of equilibrium critical phenomena, Rep. Prog. Phys. **30**, 615 (1967).
- [31] D. Laffargue, F. Bourée, B. Chevalier, T. Roisnel, and S. Bordère, Magnetic structures of the ternary stannide $\text{U}_2(\text{Ni}_{0.70}\text{Pd}_{0.30})_2\text{Sn}$, J. Alloys Compd. **271–273**, 444 (1998).
- [32] S. Mašková, L. Havela, A. Kolomiets, K. Miliyanchuk, A. V. Andreev, H. Nakotte, J. Peterson, K. Miliyanchuk, Y. Skourski, S. Yasin, S. Zherlitsyn, and J. Wosnitza, Onset of magnetic order in $\text{U}_2(\text{Ni}_{1-x}\text{Fe}_x)_2\text{Sn-H}$, J. Korean Phys. Soc. **62**, 1542 (2013).
- [33] K. Siemensmeyer, W. Wulf, H. J. Mikeska, K. Flachbart, S. Gabani, S. Matas, P. Priputen, A. Efdokimova, and N. Shitsevalova, Fractional Magnetization Plateaus and Magnetic Order in the Shastry-Sutherland Magnet TmB_4 , Phys. Rev. Lett. **101**, 177201 (2008).
- [34] J. Rossat-Mignod, G. H. Lander, and P. Burlet, in *Handbook on the Physics and Chemistry of the Actinides*, edited by A. J. Freeman and G. H. Lander (North-Holland, Amsterdam, 1984), Vol. 1, p. 462.

[35] S. Mašková, A. Kolomiets, L. Havela, A. V. Andreev, P. Svoboda, and Y. Skourski, Magnetic properties of $\text{Tb}_2\text{Pd}_2\text{In}$; single crystal study, *Solid State Phenom.* **194**, 58 (2013).

[36] Y. Shimura, T. Sakakibara, K. Iwakawa, K. Sugiyama, and Y. Onuki, Low temperature magnetization of $\text{Yb}_2\text{Pt}_2\text{Pb}$ with the Shastry–Sutherland type lattice and a high-rank multipole interaction, *J. Phys. Soc. Jpn.* **81**, 103601 (2012)

Figures

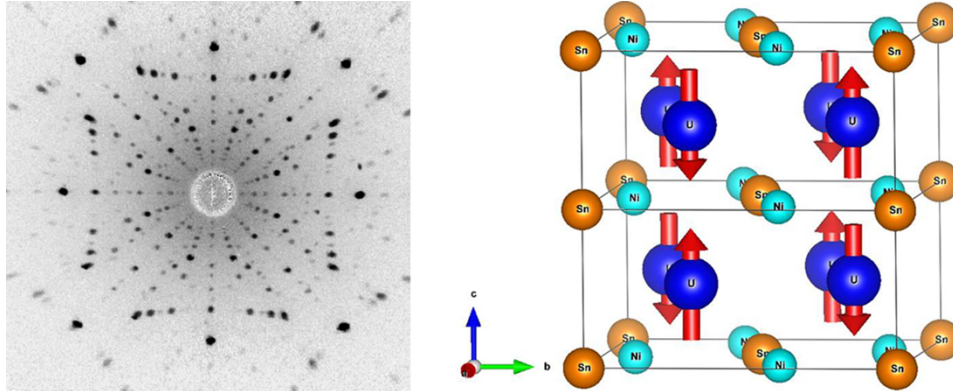


Figure 1. Laue pattern of a $\text{U}_2\text{Ni}_2\text{Sn}$ single crystal – view along the c axis (left) and the crystal structure of $\text{U}_2\text{Ni}_2\text{Sn}$ (right) with arrows showing directions of U moments, discussed below (two unit cells are shown).

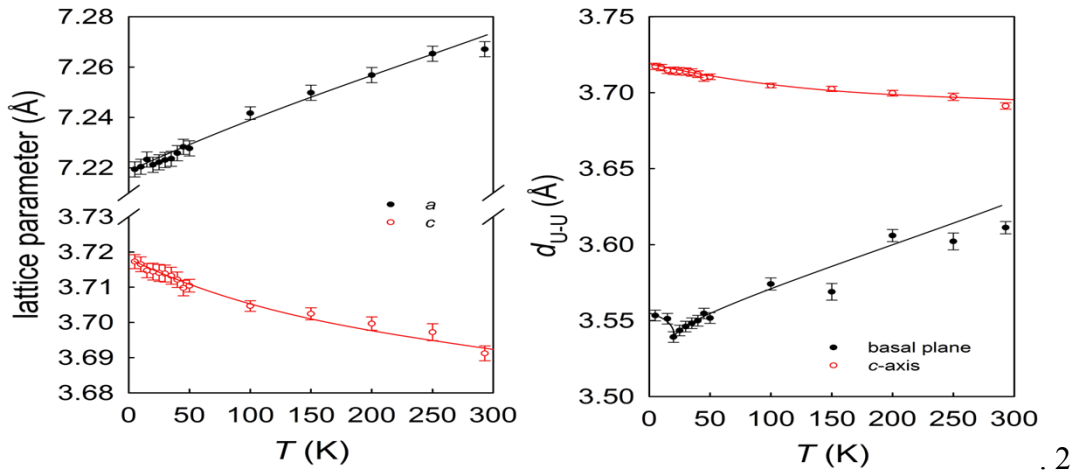


Figure 2. Temperature dependence of the lattice parameters a and c (left) and of shortest interatomic distances (right) in $\text{U}_2\text{Ni}_2\text{Sn}$ obtained from x-ray diffraction analysis.

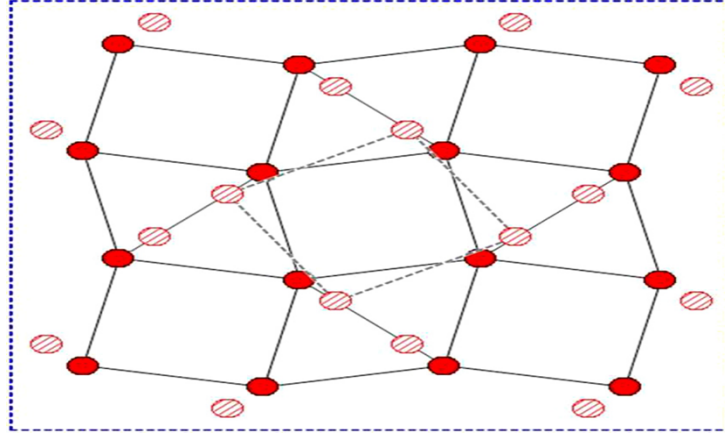


Figure 3. Schematic representation of the temperature variations of the position of U atoms in the basal plane of U_2Ni_2Sn in the paramagnetic (dashed circles) and antiferromagnetic state (full circles). It is evident that besides a contraction of a also a small rotation of the square motif (due to changing of the internal parameters x and y of the U atoms) can have impact on the shortest U-U distances.

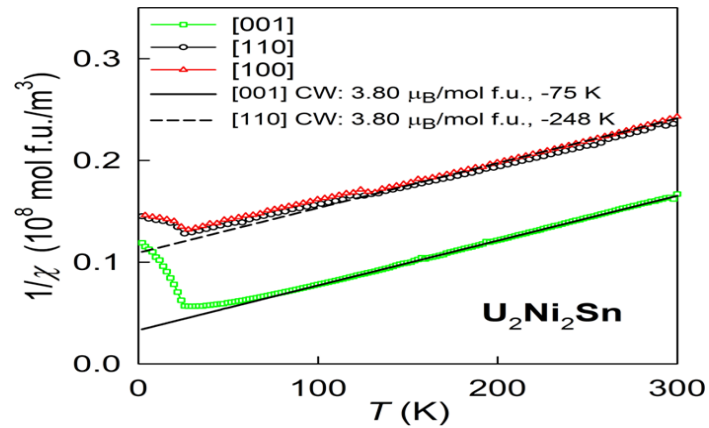


Figure 4. Temperature dependence of the inverse magnetic susceptibility of a U_2Ni_2Sn single crystal. The dashed lines are Curie-Weiss fits with parameters shown in the legends.

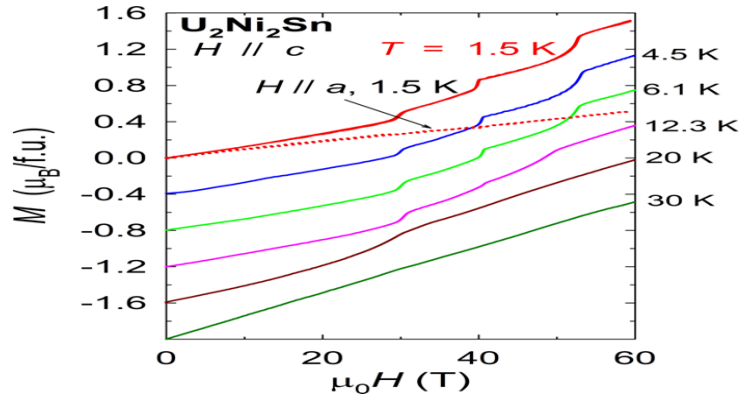


Figure 5. High-field magnetization curves with magnetic field applied along the c axis of $\text{U}_2\text{Ni}_2\text{Sn}$ single crystal at various temperatures and along the a axis (dashed line).

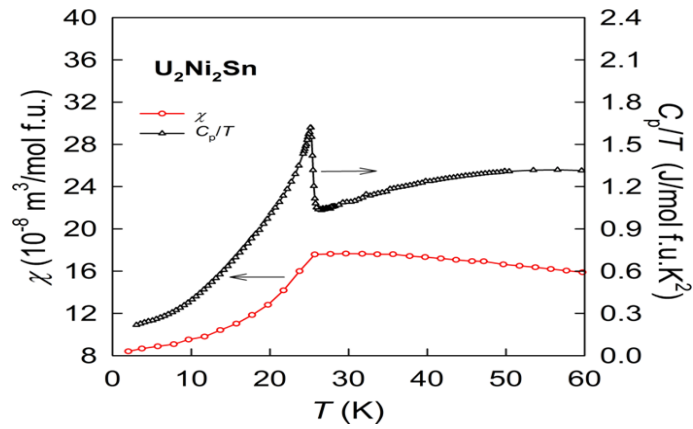


Figure 6. Detailed comparison of the temperature dependence of the magnetic susceptibility along the c axis and the specific heat in the form C_p/T (in zero field).

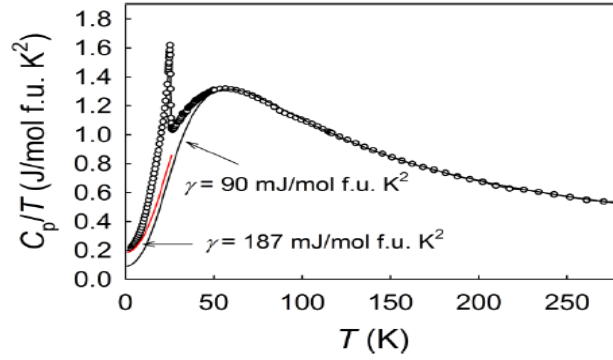


Figure 7. Temperature dependence of the specific heat of U_2Ni_2Sn compared to the specific heat calculated with the Debye temperature $\Theta_D = 207K$ for $\gamma = 90 \text{ mJ/mol f.u. K}^2$ (black line), which describes well the data in the paramagnetic state, and for $\gamma = 187 \text{ mJ/mol f.u. K}^2$, corresponding to the low-temperature γ value (red line).

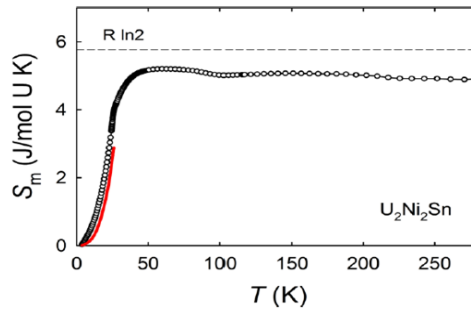


Figure 8. Magnetic entropy $S_m(T)$ per 1 mole of U atoms compared with $S = R \ln 2$ as derived by using the two types of nonmagnetic backgrounds indicated in Fig. 7.

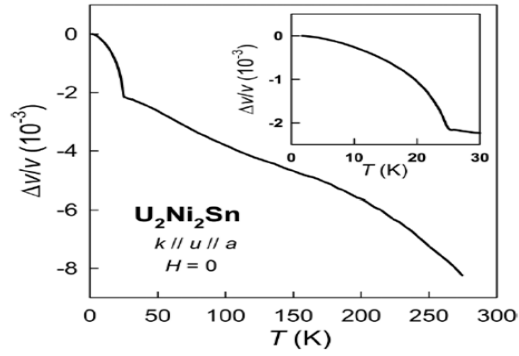


Figure 9. Temperature dependence of the ultrasound-velocity change. The inset shows the low-temperature detail.

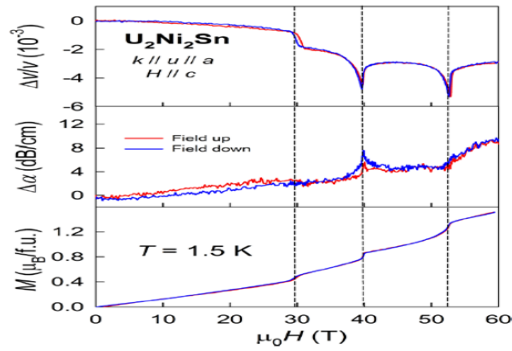


Figure 10. Field dependence of relative changes of the ultrasound velocity and attenuation compared to the magnetization of U_2Ni_2Sn measured along the c axis at $T = 1.5K$

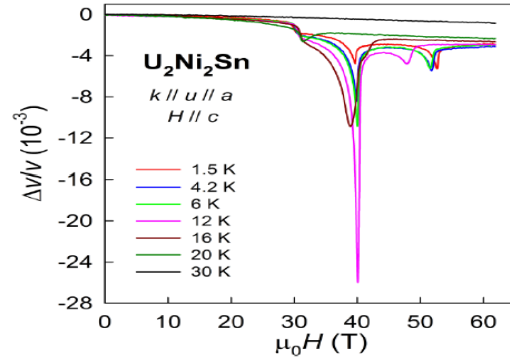


Figure 11. Field dependence of relative changes of ultrasound velocity in U_2Ni_2Sn measured along the c axis at various temperatures.

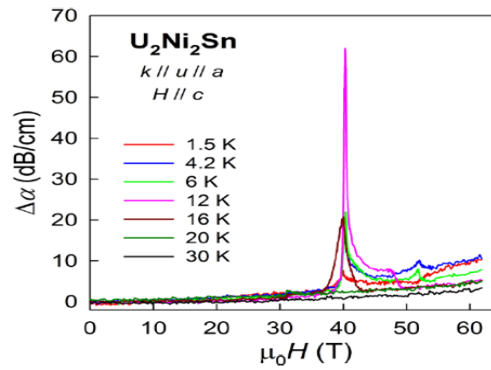


Figure 12. Field dependence of relative changes of ultrasound attenuation in U_2Ni_2Sn measured along the c axis at various temperatures.

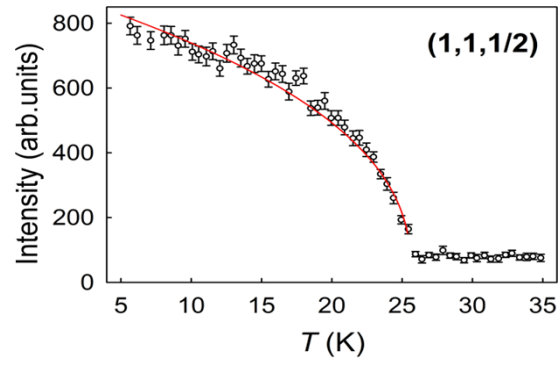


Figure 13. Temperature dependence of the intensity of the $(1\ 1\ \frac{1}{2})$ magnetic peak. The red line is the result of the fit in the whole temperature range using the expression given in the text.

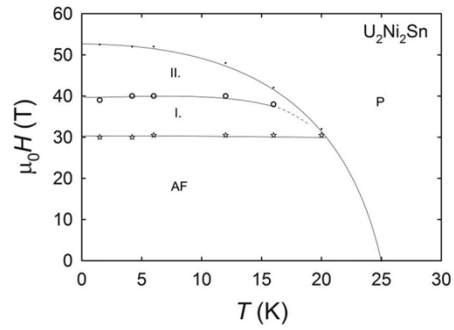


Figure 14. Tentative magnetic phase diagram of U_2Ni_2Sn .